Case Studies in Engineering Failure Analysis 4 (2015) 1–7

Contents lists available at ScienceDirect

Case Studies in Engineering Failure Analysis

journal homepage: www.elsevier.com/locate/csefa

Case study

Failure analysis of a polymer centrifugal impeller

Nikhil K. Kar [a,*], Yinghui Hu [b], Naresh J. Kar [a], Ramesh J. Kar [a]

[a] Kars' Advanced Materials, Inc., 2528W Woodland Dr, Anaheim, CA 92801, United States
[b] McGill Composites Center, Department of Chemical Engineering and Materials Science, University of Southern California, 3651 Watt Way, VHE 602, Los Angeles, CA 90089, United States

ARTICLE INFO

Article history:
Received 25 February 2015
Accepted 11 March 2015
Available online 17 April 2015

Keywords:
Failure analysis
Polymers
Wallner lines
Brittle fracture
Mirror mist hackle

ABSTRACT

A failure analysis investigation was performed on a fractured polymer impeller used in a respiratory blower. Light microscopy, scanning electron microscopy and finite element analysis techniques were utilized to characterize the mode(s) of failure and fracture surfaces. A radial split down the impeller center was observed with symmetric fracture faces about the impeller bore. Fractographic analysis revealed brittle fracture features including Wallner lines, mirror, mist and hackle features stemming from the impeller bore, emanating radially outward. Crazed fibrils and faint fatigue striations suggest that intermittent load cycling led to initiation, and rapid propagation of multiple crack fronts originating along the impeller lip. Finite element analysis revealed a flexural condition induces localized stresses along the impeller lip. Significant wear features were also observed within the impeller bore, which may have contributed to premature failure of the impeller. The brittle fracture morphology and defects within the impeller bore suggest that premature failure occurred because of multiple interacting factors including: intermittently high centrifugal velocities, imbalance bore and shaft conditions, defects within the bore caused by machining, and stress concentrations along the circumference of the impeller lip.

1. Introduction

Centrifugal pumps, compressors, and blowers utilize various impeller designs that are an essential component for bulk transport of fluids. Typically, a motor is used to spin a shaft that is connected to a housed impeller, which draws fluid in along a rotating axis. The fluid is accelerated and whirled radially and tangentially outward through the impeller vanes, where it exits through a casing designed to decelerate the fluid velocity and increase fluid pressure. Centrifugal pumps are susceptible to various modes of impeller failure including but not limited to intergranular corrosion, erosion, cavitation, material defects, as there are a number of documented case studies in the literature [1–4].

Respiratory care devices utilize centrifugal blowers for oxygen transport, which controls pressure and flow measurements for output optimization of the centrifugal blower and impeller velocity [5]. While there have been a number of failure analysis case studies related to centrifugal pumps and compressors in other industries utilizing alloy impellers, no case studies have focused on polymer based centrifugal impellers, and their associated modes of failure. Non-experimental fractographic analysis

* Corresponding author. Tel.: +1 7145277100.
E-mail address: nikhil.kar@karslab.com (N.K. Kar).

http://dx.doi.org/10.1016/j.csefa.2015.03.001

of equipment used in service allows for the understanding and further prevention of failure modes to ultimately extend the lifespan of such devices.

2. Materials and background

A failed impeller that was part of a respiratory care related blower assembly was examined to understand specific fracture features that would provide insight on reasons for failure. The blower was assembled on September 24th, 2012, and the unit was being used in a laboratory setting for testing various respiratory response scenarios. Accordingly, the unit would have been in service for just under a year, and would have seen a maximum allowable operating speed of 73,000 rpm. The FTIR spectrum (using a Nicolet Centaurus FTIR system) exhibited peaks that were characteristics of a polyetherimide polymer (as shown in Fig. 1) a high performance amorphous thermoplastic, that is used for medical devices and pharmaceutical applications. This material typically shows exceptional mechanical properties, with a yield strength of 110 MPa and retention of mechanical properties at elevated temperatures [6].

3. Fractography

Macroscopic inspection (Hirox Digital Microscope) of the impeller casing showed signs of wear on both the inner surfaces as shown in Fig. 2. Fig. 2a is an overall view of the inner casing surface where the motor is fixed in place with the mounting holes within the casing where the impeller spins. Signs of discoloration, material removal, and wear marks are shown in Fig. 2b on the alloy surface. Fig. 2c and d shows the opposite surface of the impeller casing. Visual examination showed signs of rotational wear marks and material removal of the polymer surface. While these features do indicate an imbalance condition of the impeller, it is unknown if these features were produced before or after catastrophic failure of the impeller.

Initial stereomicroscope examination of the polymer impeller indicated there were no surface defects or porosity on the exterior surface of the impeller or along the fluid vanes. The main fracture of the impeller was a radial split along a centerline, with half of the impeller remaining intact as a single piece, and the other half fracturing into multiple pieces, as shown in Fig. 3a and b. The mating fracture surfaces and the fractured remnant pieces were identified and organized to reconstruct the shape of the impeller as shown in Fig. 3a. Two symmetric fracture planes are observed in Fig. 2b. Failure of the impeller was brittle and catastrophic, showing no signs of gross plastic deformation or changes in shape when compared to a non-failed impeller as shown in Fig. 2c and d. While this polymer can elongate extensively under quasi-static loading conditions, the polymer can undergo brittle fracture, especially at elevated velocities and under high strain rate conditions in the presence of a notch/crack. The top view and side view of the non-failed impeller show a cylindrical aluminum shaft press-fit into the bore of the impeller (used to transfer the rotational motion created by the motor), and the clearance spacing between the mounting plate and bottom face of the impeller.

Microscopic examination was performed on the intact impeller half as shown in Fig. 4 using light microscopy (Hirox Digital Microscope) and scanning electron microscopy (JEOL JSM 820) techniques. Fig. 4a shows faint ridged patterns on the left half of the symmetric fracture face, curved markings that indicated the location of the fracture origin near the bottom corner, where the impeller bore was press fit against the aluminum shaft. These curved markings are identified as Wallner lines that occur under brittle fracture conditions of polymers, which can resemble fatigue striations but differ in that they represent the interaction of a stress wave with a propagating crack front [7]. The Wallner lines indicate that the nature of the

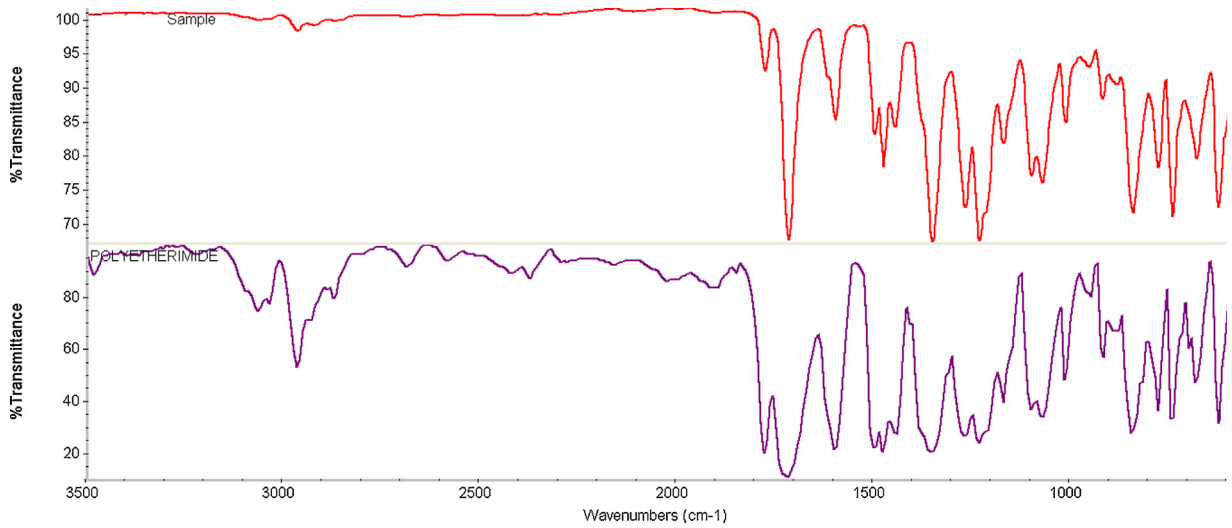

Fig. 1. Fourier transform infrared spectroscopy of impeller provides a spectrum match with library database that indicated a polyetherimide material.

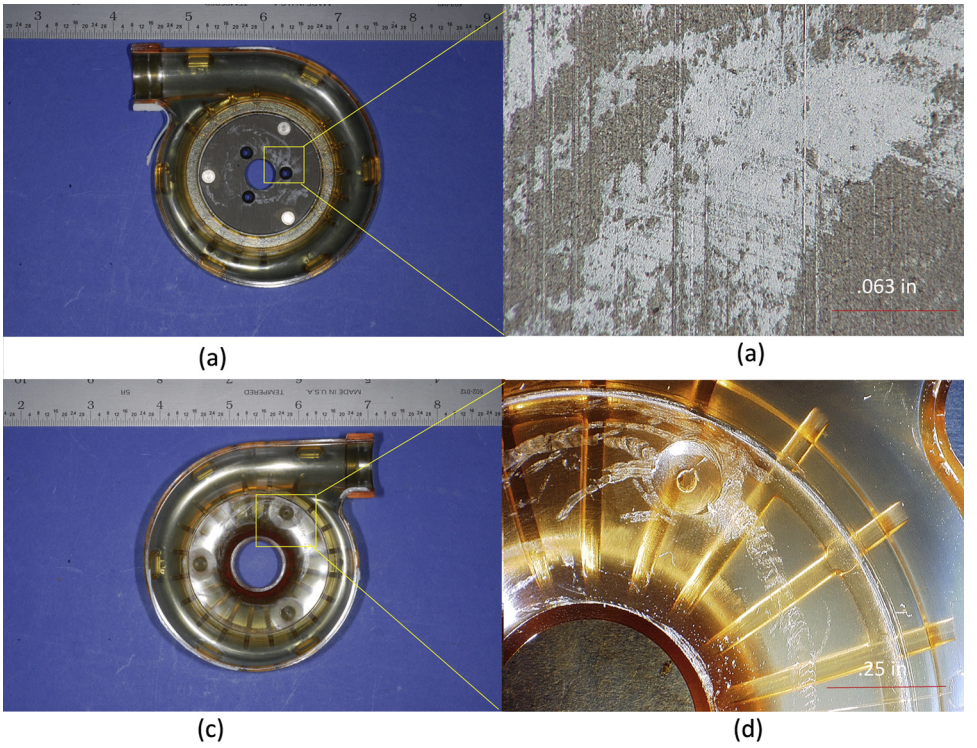

Fig. 2. (a) Overall view of impeller casing reveals signs of wear on motor mount surface. (b) High magnification view of surface shows discoloration and wear marks. (c) Polymer side of impeller casing shows rotational wear marks. (d) High magnification view of polymer casing surface shows wear evidence and material removal.

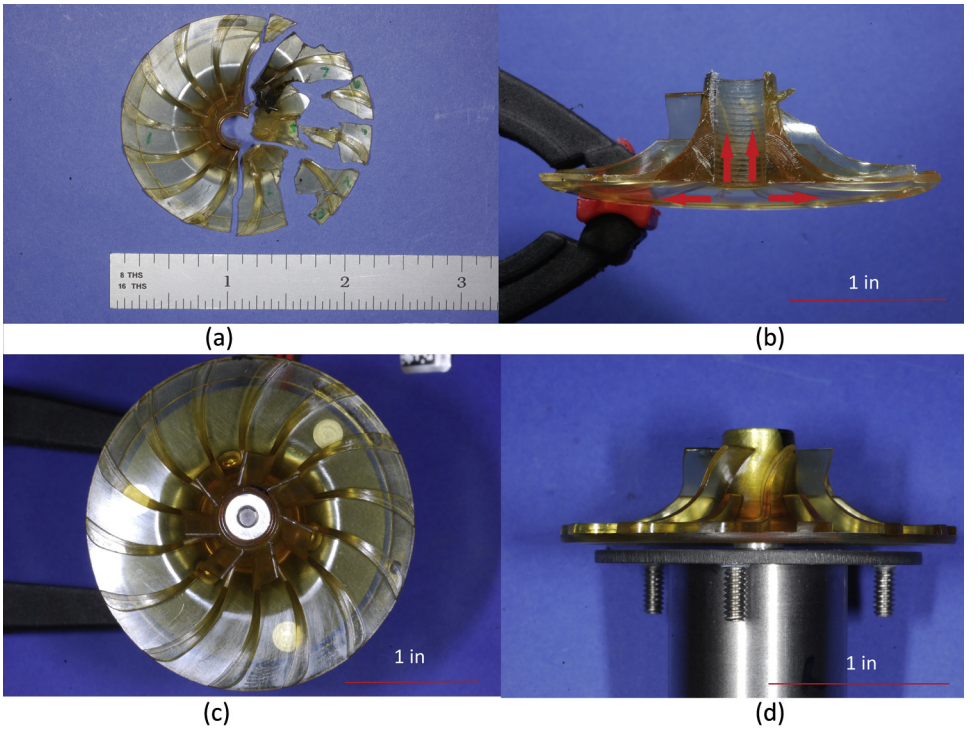

Fig. 3. (a) Overall top view of impeller fragments reconstructed for observation. (b) Image of symmetric fracture faces along the radial split of the impeller, red arrows indicate direction of crack propagation. (c) Overall top view of non-fractured impeller with aluminum shaft press fit into bore. (d) Side profile view of non-fractured impeller.

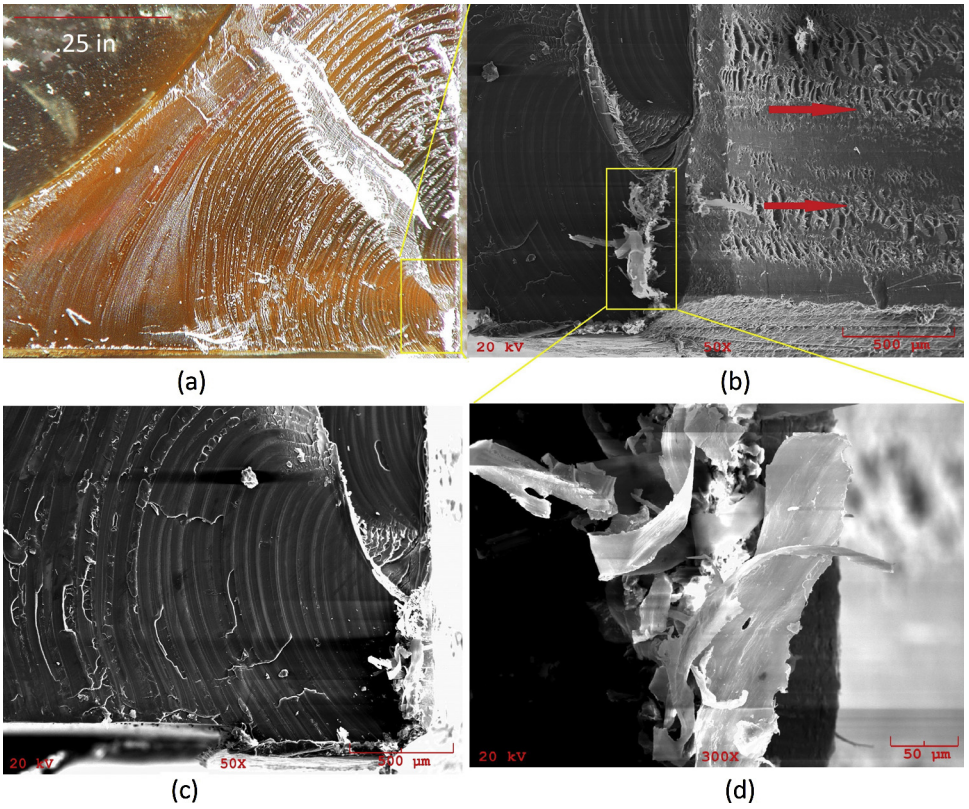

Fig. 4. (a) High magnification light microscopy image of left side fracture face reveals Wallner lines emanating from bottom corner. (b) Scanning electron microscopy image of corner shows fibril development, and defects along inner diameter bore of impeller. (c) Scanning electron microscopy image reveals transition from smooth to rough Wallner lines signifying accelerating crack front. (d) High magnification SEM image of fibril development.

failure was brittle, occurring over an extremely short time span where the curved markings were a result of an accelerating crack front interacting with a stress wave. Fig. 4b–d are high resolution SEM images of the origin, and both show multiple crack/wave interaction markings, as well as the formation of slow drawn fibrils where crazing initiated.

Drawn fibrils observed near the bottom edge of the impeller on the left half side of the fracture as shown in Fig. 4b and d. While no gross plastic deformation was observed for the impeller bulk (yielding, tearing, necking), brittle fractures of poyletherimide involve highly localized plastic flow processes that involve crazes. A craze contains an interpenetrating network of voids among polymer fibrils that bridge the craze faces [7]. The craze initiation zone shows the location of ruptured fibrils (see Fig. 4b and d) along with multiple craze fronts. As the nucleated crack grows, it forms a smooth region with signs of stress waves interacting with a propagating crack front (see Fig. 4a and c). A critical crack size is reached at which point the crack becomes unstable and propagates at a rapid rate, and this can be described by an initial mirror like region (smooth Wallner lines) as shown in Fig. 5 that transitions to portions with surface texture.

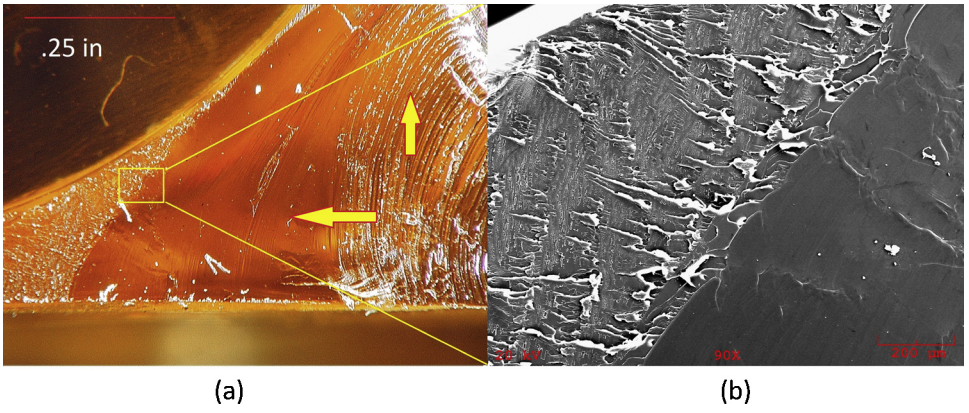

Fig. 5. (a) Light microscopy image reveals transition from Wallner lines to (b) mirror, mist and hackle morphology as crack accelerates along radial path.

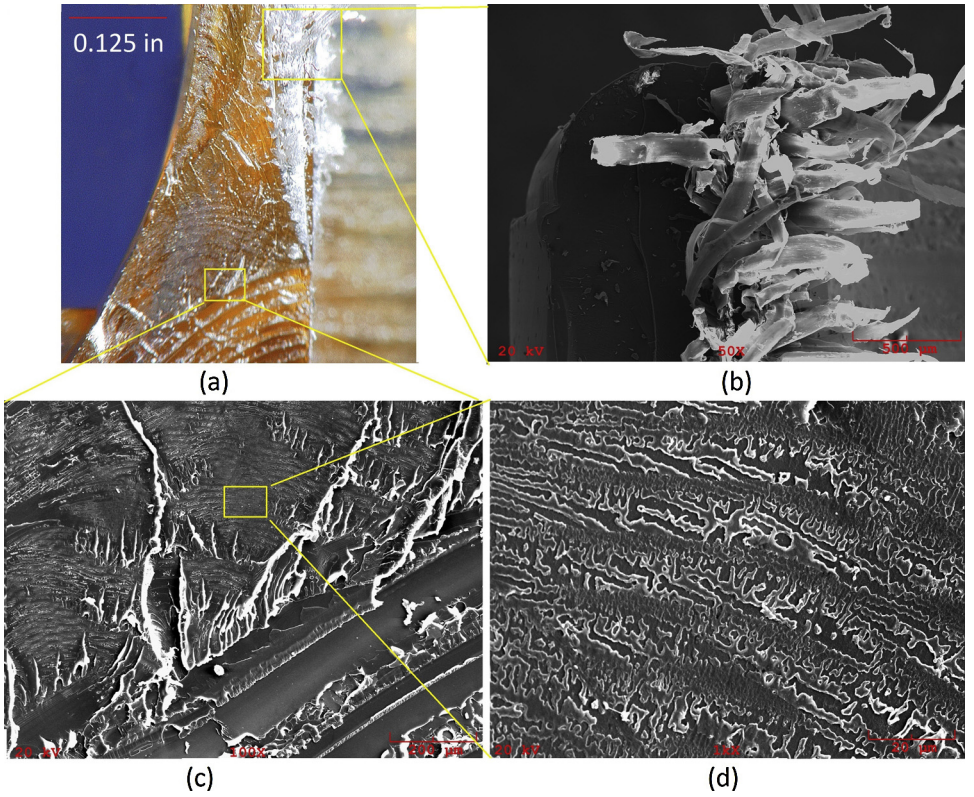

Fig. 6. (a) Light microscopy image reveals transition from Wallner lines to mist and hackle morphology and (b) formation of long fibrils. (c) Scanning electron microscopy image of transition zone shows fracture features consistent with hackles. (d) Higher magnification SEM image within hackle region shows mist formation in the form of surface undulations.

The direction of crack propagation appeared twofold based on the observed variation in fracture features. Unstable crack propagation took place from the bottom corner near the aluminum shaft and bore interface, to the outer circumference of the impeller, along a horizontal direction as shown with the arrows in Figs. 2b and 5. A transition from Wallner lines to a featureless (mirror-like) region, and then to mist/hackle ridges is shown in Fig. 5b. The transition from a featureless region to the mist and hackle region in Fig. 5b is indicative of rapid crack propagation in the polymer. Unstable crack propagation morphologies also appeared along the vertical direction, stemming the bottom corner near the aluminum shaft and bore interface to the tallest region of the inner bore as shown in Fig. 6. The images show a transition zone from rough Wallner lines in Fig. 6a and c to fracture features that have both mist/haze and hackle morphologies. The mist fracture surfaces show up as flat undulations with slight changes in surface texture. Hackle regions are particularly rough, and show outward ridges associated with final fracture when highly localized plastic deformation takes place with the formation of minute shear lips. There was also evidence of elongated fibrils near the top portion of the bore as shown in Fig. 6b, which suggests a region slow fracture, and may indicate final rupture where the impeller halves pulled apart from each other.

The symmetric fracture faces about the impeller bore as shown in Fig. 2 revealed that on both faces, the fracture morphology exhibited distinct brittle fracture features: Wallner lines, a mirror-like featureless region, and rough fracture regions. Fig. 7a and b shows the right face of the impeller half revealing these features. High resolution inspection of the failure surfaces showed Wallner lines along with mirror, mist, and hackle regions which represent the history and location of crazes that turned into an accelerating crack as a function of time. Because the impeller underwent strenuous and intermittent cyclic loading conditions, fatigue induced striations may have also play a role in the failure of this impeller. Fig. 7b shows faint striations (see red arrow) near the bottom lip which appear different from the macroscopic Wallner lines observed in Fig. 7a. No slow drawn fibrils were observed on the right fracture face, as observed on the left fracture face discussed previously.

Further investigation of the impeller showed significant signs of wear on the diameter of the impeller bore as shown in Figs. 4b (red arrows) and 7c. The morphology observed here is an indication of wear induced defects caused by a reaming operation used to press fit the aluminum shaft with the bore of the impeller. Defect size and control are important factors in preventing premature failure of polymer components under various loading conditions. Critical defects may interact concurrently with shaft misalignment, resonance, or impact situations that can lead to fatigue crack growth, inducing catastrophic failure of such polymer impellers.

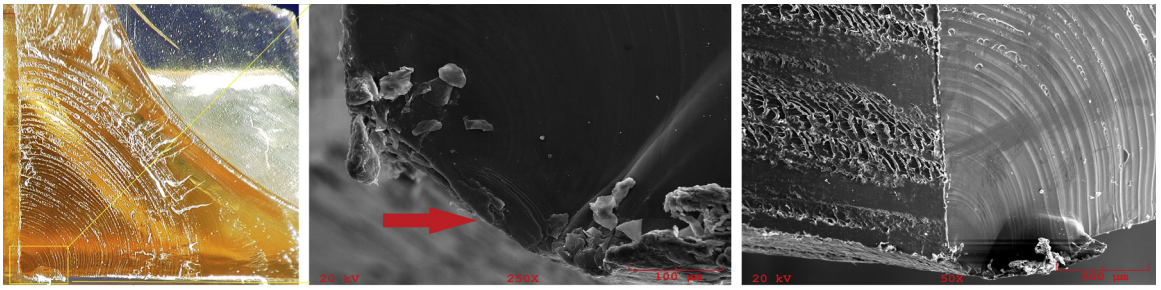

Fig. 7. (a) Light microscopy image of right side fracture face reveals macroscopic Wallner lines and location of fracture origin. (b) High magnification SEM image of fracture origin shows faint fatigue striations. (c) Oblique view of fracture origin reveals bore defects along inner diameter which could contribute to premature failure.

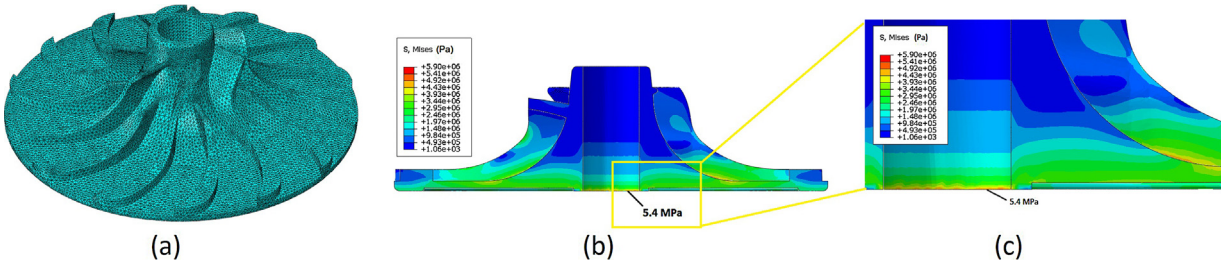

Fig. 8. (a) High density three dimensional mesh applied to impeller model. (b) Cross sectional view of impeller reveals von mises stress distribution. (c) Close up view of impeller lip reveals concentrated stresses along circumference of lip, conditions created due to flexing condition of impeller.

Table 1
Mechanical properties input.

Density (kg/m^3)	Elastic modulus (GPa)	Poisson's ratio
1107	3.42	0.33

4. Finite element analysis

Finite element analysis (FEA) was performed on the impeller under maximum centrifugal conditions (72,000 rpm including a gravitational load) to determine the locations of the highest stress. The impeller was analyzed using commercial software (Abaqus, Dassault Systèmes). Because of the complex geometry of the impeller, tetrahedral elements (C3D10) were used to mesh the model as shown in Fig. 8a. The total number of elements used was ~270,000 while the total number of nodes used was ~420,000. Air fluid interaction with the impeller vains was not taken into account because computational fluid dynamic simulations were beyond the scope of the study.

Material mechanical properties input are listed in Table 1. The material is regarded homogenous.

A boundary condition was applied to model the contact between the aluminum shaft with the impeller bore. The analysis was conducted in two steps: in the first step, gravity was applied (9.8 m/s^2), in the direction perpendicular to the bottom surface; in the second step, centrifugal force was added (72,000 rpm).

Fig. 8b and c shows the von Mises stress distribution at the cross-section under both gravity and centrifugal load. The bottom lip location within the bore shows stress concentration up to 5.4 MPa, however this stress level is much lower than the yield strength of this material (~110 MPa). The results indicate that elevated von Mises stresses exist near the bore of the impeller where the bottom lip meets the rotating shaft. Because of the bore constraint against the aluminum shaft, the bottom corners appear to act as stress concentration sites as the impeller rotates and displaces under flexural conditions. The stress concentrations coincide with the craze and fatigue initiation sites described in the previous figures. The elevated stress region combined with inner bore defects near the bottom lip increase the probability of craze/crack initiation which may have induced premature failure of the impeller.

5. Conclusion

A failed, centrifugal polyetherimide impeller was analyzed using light microscopy, scanning electron microscopy and finite element analysis to provide insight on causes for premature failure. The investigation showed symmetric brittle

fracture features which include Wallner lines, mirror, mist, and hackle zones that emanated from an origin near the base and bore of the impeller, and additionally showed signs of fretting damage that may have contributed to premature failure due to defect growth. Slow drawn fibrils were observed on the left half face of the fracture origin, while faint fatigue striations were observed near the right half face of the fracture suggesting that the right half was the primary fracture, and the left half fracture failed in a secondary fashion, with separation of the impeller into two halves creating drawn fibrils. Finite element analysis showed that centrifugal loads produced a stress concentration along the impeller lip where the fracture initiated. To increase service life and reduce the potential for premature failure, the fretting wear defects (caused by reaming) need to be minimized.

Acknowledgements

I acknowledge and thank the technical staff at Kars' Advanced Materials Inc. for their discussions and assistance (Mitch Peralta, Tim Roig, Vicente Cheng, Rohan Panikar), and CareFusion Respiratory Care (Steve Duquette, Harold Miller, and Edgardo Marcelo) for providing the samples for analysis and the helpful discussions we had.

References

[1] Das S, Mukhopadhayay G, Bhattacharyya S. Failure analysis of the impellers of coke plant. Case Stud Eng Fail Anal 2014;2:157–61.
[2] Khalid YA, Sapuan SM. Wear analysis of centrifugal slurry pump impellers. Ind Lubr Tribol 2007;59(1):18–28.
[3] Zheng YG, Hu HZ, Zhang YM, Hu HX. Failure analysis of melt pump impeller. Tribol Mater Surf Interfaces 2013;7(4):216–23.
[4] Shoushtari AA, Ranjbar K, Mousavi SM, Yancheshmeh DA. Study on failure analyses and material characterizations of a damaged booster pump. J Fail Anal Prev 2013;13(4):489–95.
[5] White G. Equipment theory for respiratory care. Cengage Learn 2014;457–9.
[6] Johnson RO, Burlhis HS. Polyetherimide: a new high performance thermoplastic resin. J Polym Sci Polym Symp 1983;70:129–43.
[7] Characterization and failure analysis of plastics. ASM Int 2003;410–5.